Direct-write fabrication of freestanding nanocomposite strain sensors

2012 Nanotechnology 23 085502

(http://iopscience.iop.org/0957-4484/23/8/085502)

Nanotechnology **23** (2012) 085502 (9pp) doi:10.1088/0957-4484/23/8/085502

Direct-write fabrication of freestanding nanocomposite strain sensors

Rouhollah Dermanaki Farahani[1], Hamid Dalir[1], Vincent Le Borgne[2], Loick A Gautier[2], My Ali El Khakani[2], Martin Lévesque[1] and Daniel Therriault[1]

[1] Laboratory for Multiscale Mechanics, Center for Applied Research on Polymers (CREPEC), École Polytechnique de Montreal, C P 6079, succ. Centre-Ville, Montreal, QC, H3C 3A7, Canada
[2] Institut National de la Recherche Scientifique, INRS-Énergie, Matériaux et Télécommunications, 1650 Boulevard Lionel-Boulet, Varennes, QC, J3X 1S2, Canada

E-mail: daniel.therriault@polymtl.ca

Received 3 November 2011, in final form 10 January 2012
Published 1 February 2012
Online at stacks.iop.org/Nano/23/085502

Abstract
This paper deals with the design and microfabrication of two three-dimensional (3D) freestanding patterned strain sensors made of single-walled carbon nanotube (SWCNT) nanocomposites with the ultraviolet-assisted direct-write (UV-DW) technique. The first sensor consisted of three nanocomposite microfibers suspended between two rectangular epoxy pads. The flexibility of the UV-DW technique enables the sensor and its housing to be manufactured in one monolithic structure. The second sensor was composed of a nanocomposite network consisting of four parallel microsprings, which demonstrates the high capability of the technique when compared to conventional photolithographic technologies. The performances of the sensors were assessed under tension and compression, respectively. The sensors' sensitivities were evaluated by correlating their measured resistivities to the applied displacements/strains. Electrical conductivity measurements revealed that the manufactured sensors are highly sensitive to small mechanical disturbances, especially for lower nanotube loadings when compared to traditional metallic or nanocomposite films. The present manufacturing method offers a new perspective for manufacturing highly sensitive 3D freestanding microstructured sensors.

(Some figures may appear in colour only in the online journal)

1. Introduction

There has been a growing interest over the past decade in the development of carbon nanotube (CNT) reinforced polymer nanocomposites, considered as realistic alternatives to conventional smart materials [1–11]. The high aspect ratio of CNTs [12] and their excellent electrical properties [13] confer electrical conductivity and sensing capability to inherently insulating polymers, which make their nanocomposites suitable for use in a broad range of potential applications such as electrostatic charge protection for aircrafts [14], sensors [2, 8, 10, 11], actuators [1, 15] and electromagnetic interference shielding [10, 14].

Among these applications, CNT-reinforced polymer nanocomposite films have been extensively used for structural health monitoring for industrial and national infrastructure [4, 5, 8]. Nanocomposite film strain sensors might be preferred over conventional metal foil strain sensors in some applications due to their enhanced electromechanical sensitivity and their ability to accurately measure large strains [16]. The electromechanical sensitivity of nanocomposite sensors stems from the rearrangement of percolating conducting pathways induced by an external mechanical disturbance. In particular, the electrical conductivity of nanocomposite films decreases with increasing mechanical strain under tension because the distances between non-contacting neighboring nanotubes are increased and/or the contact area between the nanotubes in their percolation pathways are influenced [3]. Another possible contribution may arise from the intrinsic variation of

the conductivity of CNTs due to mechanical strain, as reported in the literature [17–19]. It has been found that the nanotube concentration, dispersion and manufacturing process are the key parameters affecting the electromechanical sensitivity of such nanocomposite-based sensors. In general, the highest sensitivity is achieved when the nanotube content approaches the percolation concentration threshold where the electron tunneling between neighboring nanotubes at sufficiently close proximity is the dominant mechanism [3].

Most of the research has been limited to the use of nanocomposite films to manufacture strain sensors [5, 10, 17–19]. Nanocomposite films are limited, by nature, to only provide in-plane strain measurements. In addition, they must be bonded over their whole area and might capture undesired parasitic perturbations (local cracks, plasticity, etc) in applications where overall measurements are sought. The sensitivity of such sensors can be improved by decreasing their width and thickness [20]. However, this potential tailoring is somewhat limited by fabrication and manipulation constraints. Finally, bulk nanocomposite films cannot be patterned like traditional strain sensors consisting of a long, thin conductive strip of patterned lines. This limits further the possibilities for improving their sensitivities. Photolithographic techniques (resolution down to 120 nm [21]) could be used for manufacturing patterned nanocomposite strain sensors. This technique could also enable the fabrication of sensing elements directly on the surfaces of structures [22]. However, this technique is far from being cost-effective. Therefore, new advances in the fabrication processes are still needed to easily and cost-effectively manufacture a supported or freestanding nanocomposite strain sensor with desired two- and three-dimensional (2D and 3D) patterns.

This paper focuses on the use of the ultraviolet-assisted direct-write (UV-DW) technique recently developed in our group [23] for the fabrication of freestanding nanocomposite patterned strain sensors. The flexibility of this fabrication method enabled us to tailor and cost-effectively pattern deposited nanocomposite 2D lines like traditional strain gauges and also to fabricate two freestanding 3D-patterned strain sensors. The first manufactured freestanding strain sensor consisted of three nanocomposite microfibers suspended between two rectangular epoxy pads. The electromechanical sensitivity of the structure was evaluated under tensile loading in a dynamic mechanical analyzer (DMA) with a film tension clamp. The second sensor was composed of a square network of four parallel microsprings enclosed by two circular pads at its top and bottom. The sensitivity of this sensor was characterized in DMA with a compression clamp. The manufacturing technique presented here opens up new prospects for the achievement of cost-effective geometry-optimized nanocomposite microdevices for micro-electronics applications.

The paper is organized as follows: section 2 deals with all the experimental details including nanotube characterization with a few methods, the nanocomposite preparation procedure and viscosity characterization. This is followed by the fabrication of two freestanding nanocomposite patterned strain sensors with the UV-DW technique. All the results obtained from the experiments are discussed in section 3. This section begins with the CNTs and the viscosity characterization of their epoxy nanocomposites. Finally, the electromechanical sensitivities of the nanocomposite sensors are presented and discussed.

2. Experimental details

2.1. Nanocomposite preparation and characterization

Single-walled carbon nanotubes (SWCNTs) were synthesized by the UV–laser ablation (248 nm, 20 ns, 400 mJ) method using a Co/Ni-doped graphite target in an argon atmosphere at a temperature of 1150 °C. The as-produced SWCNTs were then subjected to a three-step chemical purification treatment (details can be found in [24, 25]) to remove the impurities like metal catalyst particles and other carbonaceous structures.

The purified SWCNTs were then used to prepare nanocomposites at different nanotube loadings by mixing them with an ultraviolet/heat curable epoxy (UV–epoxy; UV15DC80, Master Bond Inc.). The UV–epoxy used here contains a UV photo-initiator with an optimal absorption at 365 nm and a heat-initiator active in the 60–80 °C range. Non-covalent functionalization of the nanotubes using surfactant was applied to the solubilized nanotube aggregates. The desired amount of purified SWCNTs was added to a solution of 0.1 mM of zinc protoporphyrin IX (Sigma-Aldrich) in acetone. The suspension was sonicated in an ultrasonic bath (Ultrasonic Cleaner 8891, Cole-Parmer) for 90 min. The UV–epoxy was then slowly mixed with the nanotube suspension in acetone over a magnetic stirring hot plate (model SP131825, Barnstead International) at 50 °C for 4 h. The solvent was evaporated by placing the nanocomposite under a hood at room temperature for 24 h, followed by vacuum oven (RK-52402, Cole-Parmer) curing at 30 °C for 12 h and at 50 °C for 24 h. The nanocomposites were passed through a three-roll mill mixer (Exakt 80E, Exakt Technologies) for final high shear mixing upon solvent evaporation. The gaps between the rolls varied in three batch-wise processing steps including five passes at 25 μm, five passes at 10 μm and ten passes at 5 μm, respectively. The rotation speed of the apron roll was set to 250 rpm. The final mixture was then degassed under a vacuum of 0.15 bar for 24 h. The nanocomposites were stored in UV-protective 3CC syringes (Nordson EFD) at room temperature. Based on our experience, the nanocomposite materials remain stable at least for a year under the above conditions.

The purified SWCNTs were observed by transmission electron microscopy (TEM) using a Jeol JEM-2100F (FEG-TEM, 200 kV) microscope. Their Raman spectra were acquired at room temperature in the 100–2000 cm^{-1} spectral region under ambient conditions using a back-scattering geometry on a micro-Raman microscope (Renishaw Imaging Microscope Wire TM) with a 50× objective. A 514.5 nm (2.41 eV) line from an air cooled Ar+ laser was used for excitation radiation.

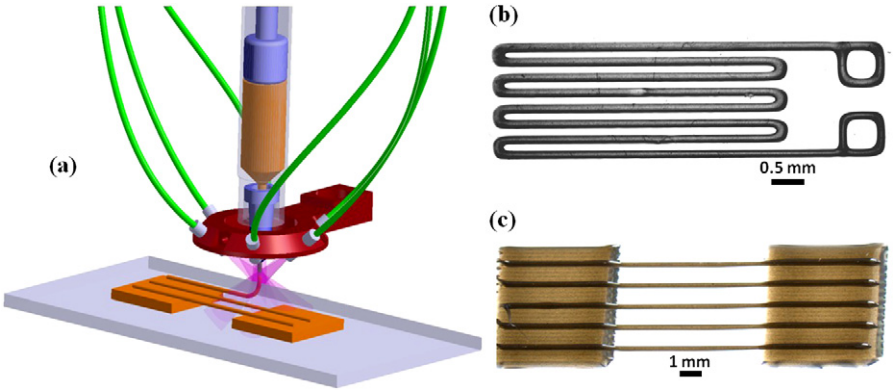

Figure 1. (a) Schematic representation of the UV-assisted direct-writing of nanocomposite microstructures. (b) A deposited line network similar to traditional strain gauges. (c) A microfiber coupon. To fabricate these microstructures using the UV-DW technique, the nanocomposite is extruded through a capillary micro-nozzle by an applied pressure and is partially cured shortly after extrusion under UV illumination.

The process-related apparent viscosity of the pure UV–epoxy and its associated nanocomposites were measured from an experimental method based on capillary viscometry [26, 27]. To obtain different shear conditions, 10 continuous filaments of material were extruded through a micro-nozzle (5132-0.25-B, precision stainless steel tips, EFD, $L =\sim 20$ mm and internal diameter (ID) $= 100$ μm) at five different pressures over glass substrates. The filaments were deposited using a computer-controlled robot (I & J2200-4, I & J Fisnar) and a fluid dispenser (HP-7X, EFD) with a calibrated deposition speed. Shortly after the deposition, the filaments were cured under UV lamp (RK-97600, Cole-Parmer) illumination for 5 min. The material flow rates were calculated from the filaments' cross-section and the extrusion speed was controlled by the dispensing apparatus. The cross-sectional area of the filaments was measured with an optical microscope (BX-61, Olympus) and image analysis software (Image-Pro Plus V5, Media Cybernetics). The process-related apparent viscosity and the process-related apparent shear rate were calculated from capillary viscometry equations including the Rabinowitsch correction.

2.2. *Fabrication of the sensors and their characterization*

The UV-DW technique was used to fabricate nanocomposite-based strain sensors. The UV-DW technique relies on a computer-controlled robot (I & J2200-4, I & J Fisnar) that moves a dispensing apparatus (HP-7X, EFD) and a UV light-emission set-up along the x-, y and z-axes. Figure 1(a) schematically represents the fabrication of different microstructures using UV-curable nanocomposite materials. The materials are photopolymerized under the illumination of UV light using two high-intensity UV light-emitting diodes (LEDs; NCSU033A, Nichia) while being extruded. The fast curing of nanocomposite materials enables the fabrication of supported or freestanding 3D structures when the extrusion position spatially changes in three dimensions. Figures 1(b) and (c) show optical images of two deposited nanocomposite microstructures with sufficient control of the resolution and patterns manufactured with this flexible, efficient and cost-effective method. In particular, the network shown in figure 1(b) was fabricated in only 20 s.

The UV-DW technique was also used to fabricate two 3D-patterned freestanding nanocomposite strain sensors. In the first sensor, three 100 μm-diameter nanocomposite microfibers suspended over an 8 mm gap between two rectangular epoxy pads were fabricated by extruding the nanocomposite suspension through a micro-nozzle (precision stainless steel tips, EFD, internal diameter $= 100$ μm). The two epoxy pads were silver-coated to ensure proper electrical contact and served as electrodes. Another layer of epoxy was subsequently deposited over the two pads using the UV-DW technique. This electrically insulated the fibers in order to reduce parasitic effects.

The second type of sensor was composed of a square network of four identical 1 mm-diameter microsprings. The microsprings were fabricated on a small circular aluminum plate in a rectangular layout having an inter-coil distance of 2 mm. Another aluminum plate was subsequently attached to the top of the springs. Electrical measurement probes were attached to the aluminum plates which served as conductive electrodes. Finally, the microfibers and the microspring networks were post-cured at 120 °C for 1 h.

The electromechanical sensitivity of the sensors was evaluated by relating both their measured electrical conductivity and strains (or displacements) as the sensors underwent mechanical loading. The electrical conductivities of the nanocomposite-based sensors were measured with a Keithley 4200 semiconductor parametric analyzer (MM 2000 probe station). The mechanical response of the strain sensors (i.e. force–displacement) was measured in a dynamic mechanical analyzer (DMA; DMA2980, TA Instruments). The microfibers were tested using a film tension clamp with a constant loading rate of 0.5 N min^{-1} to reach a maximum displacement of 1 mm. The mechanical response under compression of the microspring network was characterized with a compression fixture at a load rate of 0.5 mN min^{-1} for a maximum displacement of 3 mm.

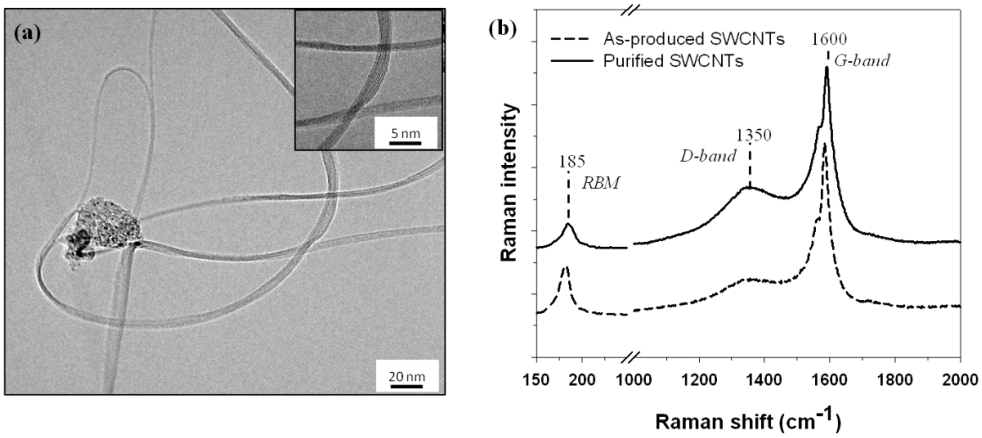

Figure 2. (a) Typical TEM images of purified SWCNTs, (b) Raman spectra of as-produced (bottom) and purified (top) SWCNTs.

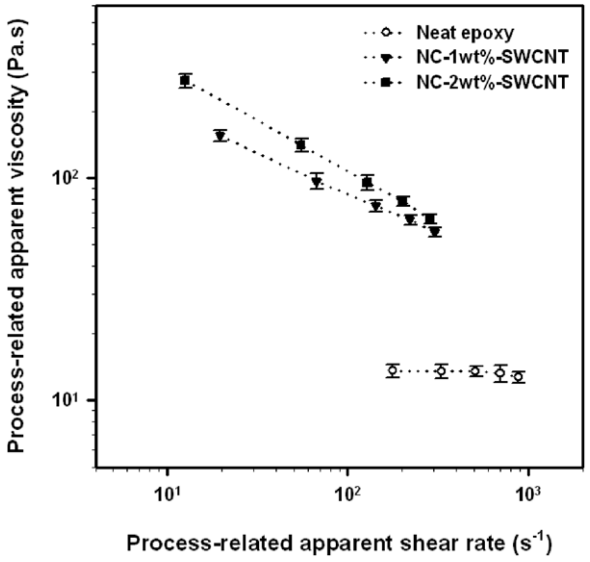

Figure 3. Process-related apparent viscosity of the neat UV–epoxy and its nanocomposites with respect to apparent shear rate using a method based on capillary viscometry. The error bars were calculated from the 95% confidence intervals on the mean value obtained from the measurements.

3. Results and discussions

3.1. Carbon nanotube characterization

Figure 2(a) A TEM micrograph of typical laser-synthesized SWCNTs after their chemical purification. The nanotubes are observed to self-organize into high aspect ratio (i.e. length/diameter) bundles (length up to 10 μm; diameter $\sim$1.24 nm). The chemical purification of the nanotubes removed any residual catalyst particles and other carbonaceous structures. However, a few dark spots are still observed. These are most probably residual catalyst nanoparticles that were not entirely digested during the nitric acid oxidation treatment.

The structure of as-produced and purified SWCNTs was characterized using Raman spectroscopy. Figure 2(b) shows typical Raman spectra of the as-produced and purified SWCNTs, representing three typical peaks for the CNTs. The spectra include a narrow radial breathing mode (RBM) band centered around 185 cm^{-1}, a D-band centered around 1350 cm^{-1} and a G-band around 1600 cm^{-1}. The RBM peak is attributed to the presence of SWCNTs with a mean diameter of 1.2 nm, in accordance with the measurements from direct TEM observations. The G-band corresponds to the symmetric vibrational tangential mode in graphite-like materials, and the D-band is as a signature of disorder and/or defects in these structures. The high G/D intensity ratio is generally used to determine the purity of the nanotubes. When the nanotubes were subjected to the purification process, their G/D intensity ratio significantly decreased in comparison to that of the as-produced mats. This is a consequence of the creation of additional structural defects in the nanotube surface during the nitric acid oxidation based purification process. However, the improved dispersion enabled by the creation of functional groups during the purification process outweighs their drawbacks with respect to nanotube conductivity [28].

3.2. Nanocomposite viscosity characterization

Material viscosity is a critical parameter in the UV-DW technique. Extruded materials of moderate to high viscosity are necessary to create stable filaments [23, 27]. Since high viscosity may limit flow through fine extrusion nozzles, shear-thinning behavior of an extruded material (i.e. a decrease of viscosity with an increase of shear forces inside the nozzle) is preferable. Figure 3 shows the process-related apparent viscosity (η_{app}) with respect to the process-related apparent shear rates ($\dot{\gamma}_{app}$) induced by the extrusion of the neat UV–epoxy and its associated nanocomposites for five extrusion pressures. A nearly constant viscosity of $\sim$12 Pa s is observed for the neat UV–epoxy, indicating a Newtonian behavior in the range of shear rates studied. The incorporation of purified SWCNTs to the neat resin resulted in a considerable increase (12-fold increase by adding 1 wt% SWCNTs) for η_{app} at $\dot{\gamma}_{app}$ low and the appearance of a shear-thinning behavior. The high aspect ratio of the CNTs, which possibly enabled the formation of a rheological percolation network and also their possible orientation during

extrusion, is thought to be responsible for the observed shear-thinning behavior [29]. The nanocomposites viscosity and shear-thinning behavior enabled the fabrication of microfiber coupons as well as microspring networks with the UV-DW technique. It should be mentioned that the viscosity of nanocomposites with nanotube loadings below 0.5 wt% was not found to be high enough for the UV-DW fabrication of such 3D sensors.

The increase in nanocomposite viscosity is also a good indicator of the dispersion quality of the nanotubes [30]. This is also supported by optical and SEM observation [31]. The achieved dispersion is the result of ultrasonication of the nanocomposite mixture combined with important shear forces induced in the three-roll mixer.

3.3. Electromechanical sensitivity of the sensors

3.3.1. Microfiber coupon. Figure 4 presents various aspects related to the electromechanical testing of the nanocomposite microfiber coupons. Figure 4(a) shows a typical optical image of microfibers. Figure 4(b) shows that the freestanding microfibers have a circular cross-section with a diameter of ∼120 μm. To avoid the failure of the microfibers during the electromechanical testing, the displacement at breakage was measured and found to be ∼1.5 mm (corresponds to ∼0.19 of tensile strain). Therefore, the tensile testing was stopped when the displacement reached a maximum of 1 mm. Figure 4(c) shows the force–displacement curves obtained for the nanocomposite microfibers for the range of displacements studied (average of five specimens for each fiber type). The nanocomposite microfibers for both nanotube loadings exhibit a non-linear response. This behavior might be due to the possible toughening effect of the nanotubes [32] since the response of neat epoxy resins is linearly elastic. The rigidity (i.e. tangent of curves in their linear parts) of the nanocomposite microfibers containing 1 wt% SWCNTs was found to be ∼4.7 N mm^{-1}, and increased to ∼6.3 N mm^{-1} (about 34% increase) for the fibers reinforced with 2 wt% SWCNTs. This might be attributed to the potentially high elasticity of SWCNTs, their proper dispersion and their possible beneficial orientation that may occur during the extrusion of the nanocomposite through the micro-nozzle.

Figures 4(d) and (e) show the current with respect to applied voltage (I–V) curves for the nanocomposite microfibers measured at three different strains and for nanotube loadings of 1 wt% and 2 wt%, respectively. Table 1 lists the electrical conductivities of the microfibers for five different strains. Nearly linear responses were observed for all nanocomposite microfibers within the voltage range investigated. Increase in nanotube content increased the electrical conductivity of the microfibers and also decreased their electromechanical sensitivity, as listed in table 1. Electromechanical sensitivity is usually represented as gauge factor defined as the ratio of relative resistance variation over strain variation. Higher nanotube loadings enhance the probability of contact points through which electrons are transferred and also decrease the distance of adjacent nanotubes [4, 16]. As a result, electrical conductivity is less susceptible to strain at higher nanotube loadings. Large values of the gauge factors were obtained despite the relatively high nanotube concentrations when compared to those reported in the literature [4, 5, 8]. This might be attributed to the proper nanotube dispersion and also the small microfiber diameters since gauge factor is strongly influenced by nanocomposite geometry. These values could be improved still further by decreasing the nanotube loadings close to the percolation concentration threshold, which was measured to be ∼0.2 wt% SWCNTs. Finally, figure 4(f) shows the resistivity variation of the microfibers as a function of applied tensile strain. The non-linearity of the curves might be due to separation of neighboring nanotubes through which electron tunneling is compromised [3].

The microfiber coupons could be used as real tensile strain sensors. The epoxy adhesive pads enable attachment of the sensor to a structure (figure 4(g)) while the freestanding geometry excludes any parasitic effects (local buckling) between the two ends. The geometry of the sensor can be easily tailored, depending on the application, to either sense tensile local strains (e.g. short microfibers) or overall strains (e.g. long microfibers like neurons). The diameter and number of microfibers also can be controlled by the extrusion nozzle and the deposition robot. Interestingly, the sensor can be fabricated directly on the structure using the flexible UV-DW technique. However, direct deposition of the sensor elements is possible only if the thickness of structures is less than 50 mm (i.e. the maximum distance between the extrusion nozzle and the deposition platform of the deposition robot). It is worth noting that the microfiber sensor may find other applications such as a force sensor to measure small tension loads.

3.3.2. Microspring network. Microspring networks were manufactured with the aim of fabricating a freestanding strain sensor capable of sensing out-of-plane strains. Figure 5 presents various aspects related to the electromechanical testing of the nanocomposite microspring networks. Figure 5(a) shows a SEM image of a typical network consisting of four identical springs with five coils. The first and last coils were flat in order to attach the aluminum pads for electromechanical testing. The final sensor geometry is shown in figure 5(b). The springs were arranged in a rectangular array for structural stability. The geometry of the manufactured springs matched the programmed robot's paths, which shows the high fidelity of the UV-DW fabrication technique. Figure 5(c) is a representative SEM image of the nanocomposite filament surface. The diameter of the filament was ∼130 μm, which is larger than that of the extrusion nozzle due to material swelling.

Figure 5(d) shows force–displacement curves achieved for the microspring networks under compression. The specific rigidity of the networks was increased (by 28%) with the increase of SWCNT loading to 2 wt%. Similar to the microfiber tensile experiments, the current was measured under applied voltage between two aluminum pads (top and bottom of the network) at seven different displacements as shown in figures 5(e) and (f) (only the curves for three

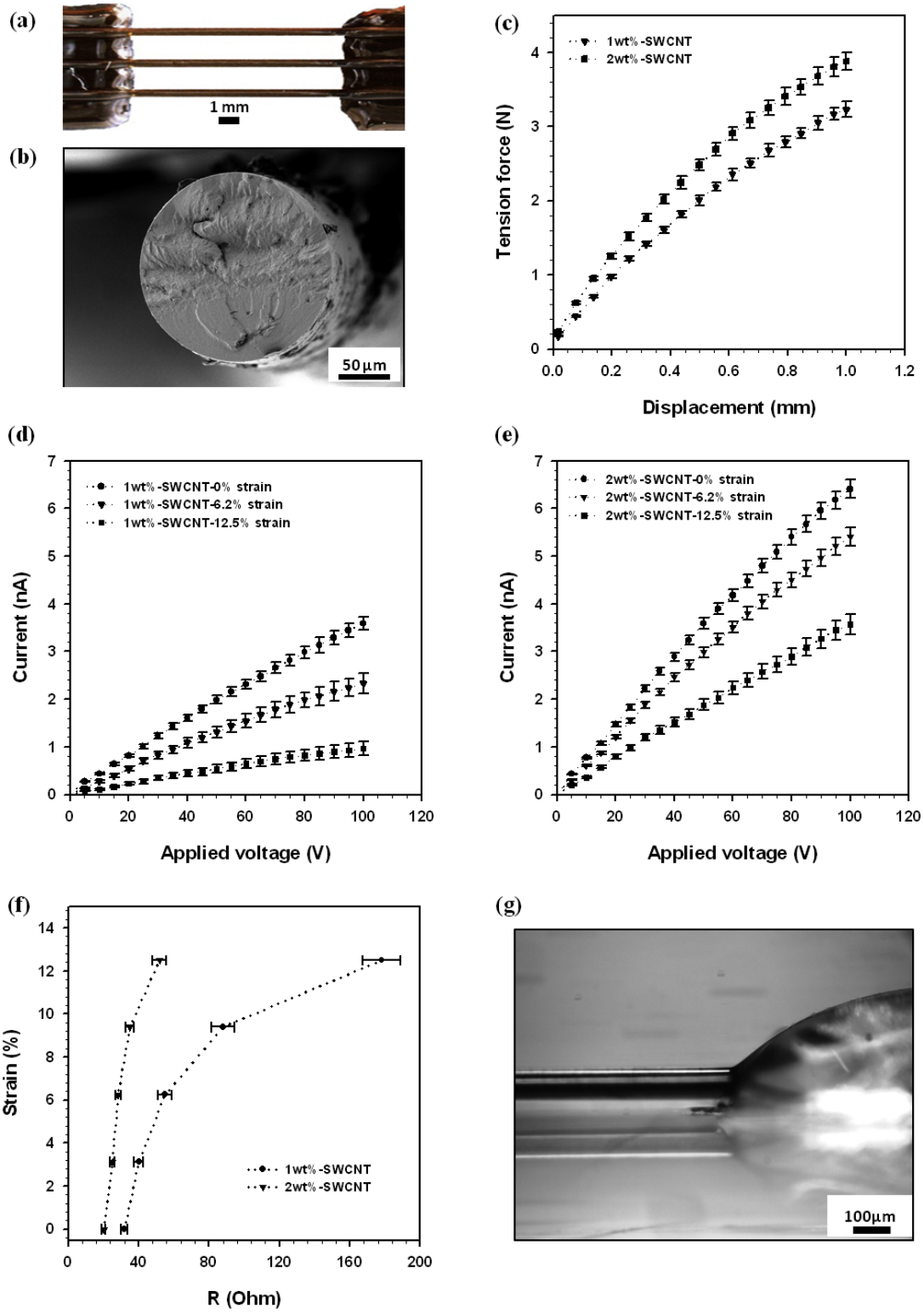

Figure 4. Electromechanical characterization of the nanocomposite microfibers under tensile strain. (a) Optical image of a typical fabricated specimen consisting of three suspended fibers between two rectangular pads. (b) SEM image of fracture surface of a nanocomposite fiber. (c) Typical force–displacement curves. (d), (e) Measured current upon voltage application between two pads for the nanocomposite microfibers respectively at 1 wt% and 2 wt% SWCNTs loadings. (f) Strain–resistivity correlated curves based on electrical resistivity changes. (g) An optical image of a microfiber coupon adhered to a structure from the pads. The error bars were calculated from the 95% confidence intervals on the mean value obtained from the measurements.

displacements are shown) for different nanotube loadings used. Table 2 summarizes the electrical conductivity of the springs for different displacements under compressive loads. As for microfibers, a linear relationship is obtained. The electrical conductivity of the microspring network increased under compressive displacements. This might be due to

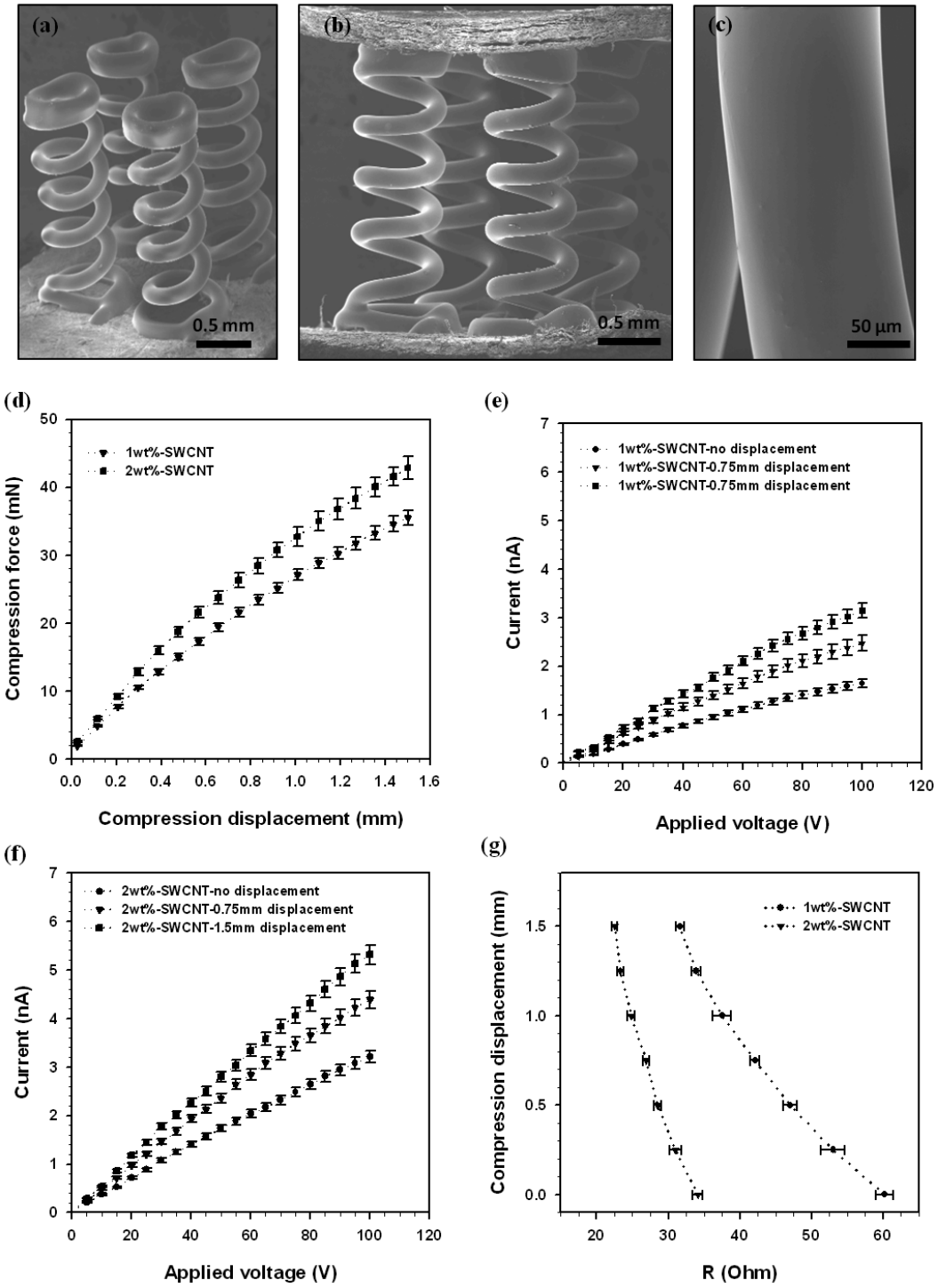

Figure 5. Electromechanical characterization of nanocomposite microsprings. (a) SEM image of a typical fabricated specimen consisting of four freestanding microsprings. (b) SEM image of the final configuration of the sensor (a circular pad on the top). (c) Filament surface SEM image. (d) Typical force–displacement curves. (e), (f) Measured current upon voltage application between two aluminum pads for the nanocomposite microfibers, respectively at 1 wt% and 2 wt% SWCNTs loadings. (g) Displacement–resistivity correlated curves based on electrical resistivity changes for the microspring network. The error bars were calculated from the 95% confidence intervals on the mean value obtained from the measurements.

the increased probability of SWCNTs being in contact, facilitating electron transfer.

Figure 5(g) shows the electromechanical sensitivity of the microspring network. The results show that gauge factors of 3.1 and 2.2 were obtained for the sensor with 1 wt% and 2 wt% nanotube loadings, respectively. These values could be improved by optimizing the number and diameter of coils and the filament diameter as well as the nanotube concentration. The desired spring geometry could be easily programmed and fabricated using the UV-DW

Table 1. Electrical conductivity changes for the microfibers under applied strains.

	Electrical conductivity at different strain (S cm^{-1})					
Strain (%)	0	3.1	6.2	9.4	12.5	Gauge factor
1 wt% SWCNTs	1.1×10^{-6}	9.4×10^{-7}	7.1×10^{-7}	4.8×10^{-7}	2.8×10^{-7}	22
Variation (±)	5.1×10^{-8}	2.8×10^{-8}	2.9×10^{-8}	1.9×10^{-8}	1.1×10^{-8}	±0.88
2 wt% SWCNTs	2.0×10^{-6}	1.9×10^{-6}	1.7×10^{-6}	1.4×10^{-6}	1.0×10^{-6}	7
Variation (±)	8.0×10^{-8}	8.3×10^{-8}	8.5×10^{-8}	7.0×10^{-8}	3.4×10^{-8}	±0.47

Table 2. Electrical conductivity changes for the microspring network under applied displacements.

	Electrical conductivity at different displacements (S cm^{-1})						
Displacement (mm)	0	0.25	0.5	0.75	1	1.25	1.5
1 wt% SWCNTs	9.9×10^{-7}	1.0×10^{-6}	1.2×10^{-6}	1.5×10^{-6}	1.6×10^{-6}	1.8×10^{-6}	2.0×10^{-6}
Variation (±)	2.9×10^{-8}	3.2×10^{-8}	3.1×10^{-8}	4.5×10^{-8}	4.4×10^{-8}	5.2×10^{-8}	5.3×10^{-8}
2 wt% SWCNTs	1.9×10^{-6}	2.0×10^{-6}	2.3×10^{-6}	2.6×10^{-6}	2.8×10^{-6}	3.0×10^{-6}	3.2×10^{-6}
Variation (±)	6.2×10^{-8}	7.1×10^{-8}	6.3×10^{-8}	7.8×10^{-8}	8.4×10^{-8}	8.1×10^{-8}	9.7×10^{-8}

technique. Although this technique enables us to fabricate longer springs, this type of sensor cannot be used for large structures because of fabrication limitations. The microspring network sensor could be used as a potential accurate scale to measure very small weights and find other applications in micro-electromechanical systems.

Lower electromechanical sensitivities were achieved for the microspring network when compared to the microfibers. This might be attributed to the different geometries of the two manufactured sensors, which possibly led to different electromechanical mechanisms. Another contribution might stem from different electromechanical mechanisms for the nanocomposite under tension and compression. As reported in the literature [6, 7], it is more challenging to bring neighboring nanotubes into contact than to increase their distance apart. The reasons discussed here are hypotheses and further work is needed to accurately quantify the sources explaining the differences in electromechanical sensitivities.

4. Conclusions

Two 3D-patterned freestanding nanocomposite strain sensors were manufactured with a UV-DW technique. The electromechanical sensitivities of the nanocomposite-based sensors were evaluated under tension and compression. A sufficient control of the sensor geometries provided by patterning small-diameter nanocomposite microfibers enabled us to reach a fairly high electromechanical sensitivity (i.e. gauge factor ∼22). Additionally, the results are thought to be more reliable since the freestanding geometry of the sensors may reduce the effect of undesirable stimulus on the results. Higher sensitivity might be achieved at lower nanotube loadings close to their percolation threshold. The contribution of the geometry, such as smaller diameter, could be easily maximized using the flexible UV-DW technique. Since the strain sensors manufactured here are examples of 3D MEMS sensors, any other complex pattern for sensing components or other applications in micro-electronics such as electromagnetic shielding could be manufactured using this technique.

Acknowledgments

The authors acknowledge financial support from FQRNT (Le Fonds Québécois de la Recherche sur la Nature et les Technologies). Professor El Khakani acknowledges also financial support from NSERC (National Science Engineering Research Council of Canada) and Plasma-Québec (le Réseau Stratégique du FQRNT sur la Science et Technologies des Plasmas). The authors would like to acknowledge the technical support of Dr B Aissa from INRS and also Dr K Laaziri from Laboratoire de Recherche sur les Nanostructures et Interfaces Conductrices for the electrical measurements.

References

[1] Li C, Thostenson E T and Chou T-W 2008 *Compos. Sci. Technol.* **68** 1227
[2] Culpepper M L and Cullinan M A 2010 *Phys. Rev.* B **82** 115428
[3] Hu N, Karube Y, Yan C, Masuda Z and Fukunaga H 2008 *Acta Mater.* **56** 2929
[4] Hu N, Yin G, Karube Y, Liu Y L, Li Y and Fukunaga H 2011 *J. Compos. Mater.* **45** 1315
[5] Zhang W, Suhr J and Koratkar N 2006 *J. Nanosci. Nanotechnol.* **6** 960
[6] Kang I, Schulz M J, Kim J H, Shanov V and Shi D 2006 *Smart. Mater. Struct.* **15** 737
[7] Kchit N and Bossis G 2009 *J. Phys. D: Appl. Phys.* **42** 105505
[8] Pham G T, Park Y B, Liang Z, Zhang C and Wang B 2008 *Composites* B **39** 209
[9] An G, Na N, Zhang X, Miao Z, Ding K and Liu Z 2007 *Nanotechnology* **18** 435707
[10] Park Y B, Pham G T, Liang Z, Zhang C and Wang B 2008 *Composites* B **39** 209
[11] Schulte K, Schueler R and Joshi S P 2001 *Compos. Sci. Technol.* **61** 921

[12] Bethune D S, Kiang C H, Devries M S, Gorman G, Savoy R and Vazquez J 1993 *Nature* **363** 605
[13] Tans S J, Devoret M H, Dai H J, Thess A, Smalley R E and Geerligs L J 1997 *Nature* **386** 474
[14] Baughman R H, Zakhidov A A and de Heer W A 2002 *Science* **297** 787
[15] Ashrafi B, Hubert P and Vengallatore S 2006 *Nanotechnology* **17** 4895
[16] Murugaraj P and Mainwaring D 2011 *Electron. Funct. Nanocompos.* **23** 549
[17] Singh G, Rice P and Mahajan R L 2007 *Nanotechnology* **18** 475501
[18] Stampfer C, Helbling T, Obergfell D, Schoberle B, Tripp M K and Jungen A 2006 *Nano Lett.* **6** 233
[19] Stampfer C, Jungen A and Hierold C 2006 *IEEE Sensors J.* **6** 613
[20] Murugaraj P, Mainwaring D E and Mora-Huertas N 2009 *Compos. Sci. Technol.* **69** 2454
[21] Kawata S, Sun H B, Tanaka T and Takada K 2001 *Nature* **412** 697
[22] Meeusen W, Clijnen J, Reynaerts D, Van Brussel H and Puers R 2003 *IEEE Sensors J.* **3** 632
[23] Lebel L L, Aissa B, El Khakani M A and Therriault D 2010 *Adv. Mater.* **22** 592
[24] Braidy N, El Khakani M A and Botton G A 2002 *Carbon* **40** 2835
[25] Le Borgne V, Aissa B, Mohamedi M, Kim Y A, Endo M and El Khakani M A *J. Nanopart. Res.* **13** 5759
[26] Bruneaux J, Therriault D and Heuzey M C 2008 *J. Micromech. Microeng.* **18** 11
[27] Lebel L L, Aissa B, El Khakani M A and Therriault D 2010 *Compos. Sci. Technol.* **70** 518
[28] Hobbie E K, Obrzut J, Kharchenko S B and Grulke E A 2006 *J. Chem. Phys.* **125** 4
[29] Rahatekar S S, Koziol K K K, Butler S A, Elliott J A, Shaffer M S P and Mackley M R 2006 *J. Rheol.* **50** 599
[30] Thostenson E T and Chou T W 2006 *Carbon* **44** 3022
[31] Farahani D R, Dalir H, Aissa B, El Khakani M A, levesque M and Therriault D 2011 *Composites* A **42** 1910
[32] Gojny F H, Wichmann M H G, Fiedler B and Schulte K 2005 *Compos. Sci. Technol.* **65** 2300